Charge Transfer Across Oxide Interfaces Probed by in Situ X-ray Photoelectron and Absorption Spectroscopy Techniques

Christian Lenser,*[,†,⊥] Qiyang Lu,[‡] Ethan Crumlin,[§] Hendrik Bluhm,[‖] and Bilge Yildiz*[,†,‡]

[†]Department of Nuclear Science and Engineering and [‡]Department of Materials Science and Engineering, Massachusetts Institute of Technology, 77 Massachusetts Avenue, Cambridge, Massachusetts 02139, United States

[§]Advanced Light Source, 1 Cyclotron Road, Berkeley, California 94720, United States

[‖]Chemical Sciences Division, Lawrence Berkeley National Laboratory, Berkeley, California 94720, United States

Ⓢ Supporting Information

ABSTRACT: The interface between two functional oxide materials governs the physical, chemical, and electronic interactions between the two phases. We investigate the charge transfer across the interface between two structurally related material classes, namely, perovskite and Ruddlesden−Popper-type oxides, choosing $La_{0.8}Sr_{0.2}CoO_{3−\delta}$ (LSC) and $Nd_2NiO_{4+\delta}$ (NNO) as our model systems for the two classes, respectively. The interface of $Nd_2NiO_{4+\delta}$ and $La_{0.8}Sr_{0.2}CoO_{3−\delta}$ is investigated using in situ photoemission spectroscopy techniques on epitaxial thin films. A detailed analysis of the electronic structure with X-ray photoelectron spectroscopy and X-ray absorption spectroscopy under an oxygen atmosphere and at elevated temperature reveals charge transfer from $La_{0.8}Sr_{0.2}CoO_{3−\delta}$ into $Nd_2NiO_{4+\delta}$. Through the use of electrical conductivity relaxation, it is demonstrated that such charge transfer from LSC into NNO is accompanied by a reduction in the kinetics of oxygen exchange on $Nd_2NiO_{4+\delta}$, contrary to expectation. Fermi level pinning at the surface of $Nd_2NiO_{4+\delta}$ is discussed as a possible cause for this phenomenon. These insights add to the understanding of material interaction necessary for the design of next-generation high-performance electrochemical components.
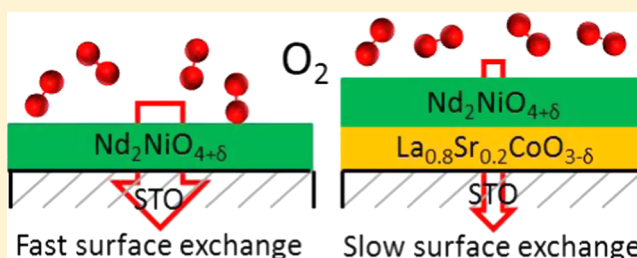
INTRODUCTION

The interface between two oxide phases has become a focal point of oxide material engineering because the interaction between the two materials allows us to tailor material properties through strain,[1] charge transfer,[2] or even emergent phenomena.[3] Recent findings include improvements in key properties such as ionic conductivity,[4] surface kinetics for oxygen reduction,[5] and the two-dimensional electron gas at the $LaAlO_3/SrTiO_3$ (STO) interface and related phenomena.[3] In particular, solid oxide electrochemical devices such as fuel cells, electrolyzers, or batteries stand to gain from improved reaction kinetics at the electrodes.[5,6]

A number of recent investigations describe improvements of the oxygen reduction reaction (ORR) kinetics, as expressed in the surface oxygen exchange coefficient, k^q, through the combination of the high-performance perovskite cathode material $La_{1−x}Sr_xCoO_{3−\delta}$ (LSC113) and its Ruddlesden−Popper (RP) phase ($n = 1$) $(La,Sr)_2CoO_{4+\sigma}$ (LSC214).[5,7,8] On the basis of investigations with scanning tunneling microscopy (STM) at elevated temperatures and in an oxygen atmosphere, our group recently suggested a model explaining the enhanced ORR activity of the heterointerface of LSC113/LSC214 centered around the exchange of electronic charge carriers and oxygen defects[9] and demonstrated the improved performance of vertically aligned nanostructured composite cathodes with respect to oxygen reduction.[10] Although the

STM investigations clearly demonstrate temperature-reversible changes in the band gap of LSC214, the mechanism of charge transfer remains under discussion. Furthermore, interdiffusion of the A-site cations has also been suggested as a possible mechanism of the ORR enhancement.[11]

This paper presents evidence of reduced oxygen exchange kinetics on the surface of a heterostructure consisting of $Nd_2NiO_{4+\delta}$ (NNO) and $La_{0.8}Sr_{0.2}CoO_{3−\delta}$ (LSC) compared to that on a single epitaxial layer. As such, the paper aims to further the understanding of charge transfer across perovskite/RP interfaces and the consequences for the kinetics of oxygen reduction. To extend our understanding beyond that of similar investigations,[12] we investigate the perovskite/RP interface using in situ X-ray absorption spectroscopy (XAS) and X-ray photoelectron (PE) spectroscopy (XPS) at resonant excitation of the B-site transition metal $L_{2,3}$ edge (resonant photoelectron spectroscopy (RESPES)) of LSC/NNO so that the spectral contributions of both layers can be clearly separated, in contrast to that in the LSC113/LSC214 system. Although NNO is itself an interesting material for the oxygen electrode of electrochemical energy conversion devices,[13,14] one central aspect to the topic at hand is whether the increased ORR activity can be

observed at an NNO/perovskite interface in analogy to the LSC113/LSC214 system. After providing evidence of reduced ORR kinetics at the surface of NNO/LSC heterostructures, we specifically address the electronic structure of LSC/NNO and NNO/LSC bilayers on single-crystalline, insulating substrates under an oxygen atmosphere and at elevated temperatures, to examine the charge transfer taking place across the interface between the two oxides.

■ EXPERIMENTAL SECTION

Epitaxial thin films of LSC and NNO were grown on single-crystalline, (001)-oriented $SrTiO_3$ (STO) single crystals (MTI, CA) by pulsed laser deposition using a KrF excimer laser to ablate the oxide targets. Deposition conditions were chosen as a temperature of 700 °C (heater setpoint), pO_2 of 10 mTorr, a laser pulse energy of 400 mJ, and a repetition rate of 5 Hz for LSC and 3 Hz for NNO. The thickness of the bilayer samples was chosen as 5 nm for the top layer and 20 nm for the bottom layer, such that the top layer is thick enough to block photoelectrons from the bottom layer, yet thin enough to allow secondary electron (SE) emission from the bottom layer for XAS. Figure 1 shows a schematic overview of the sample setup,
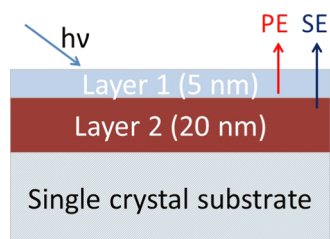

Figure 1. (a) Schematic view of the sample setup for photoemission experiments. The 5 nm thin top layer is thick enough to block photoelectrons (PEs) from the underlying layer, yet thin enough to allow the detection of secondary electron (SE) emission for XAS from the bottom layer.

and Figure S1a,b (see Supporting Information) shows exemplary X-ray diffraction and X-ray reflectivity patterns. Figure S2a,b (see Supporting Information) demonstrates that although no Ti 2p photoelectrons can be detected through 5 nm LSC films, it is possible to record XAS spectra at the Ti $L_{2,3}$ edge.

In situ XAS and XPS experiments were conducted at beamline 11.0.2 of the Advanced Light Source (Berkeley, CA) at the ambient pressure photoemission spectroscopy endstation and using monochromatic X-rays with an energy ($h\nu$) between 735 and 985 eV. XAS spectra were collected using secondary electrons with a kinetic energy of E_{kin} = 78 eV as the signal, with the analyzer set to a pass energy of 100 eV. The angle of incidence is about 15° with respect to the surface normal of the sample, and the detection angle is about 40° with respect to the surface normal. No dedicated equilibration time was allowed after a change of pO_2, but due to the necessary calibration and alignment for each step, the samples typically had 20−30 min to equilibrate before the measurements.

Modeling of the Co and Ni L edges was performed using the charge transfer multiplet (CTM) for X-ray absorption spectroscopy (CTM4XAS) software package.[15] Spectra of the Co^{3+} and Co^{2+} edges were modeled with octahedral symmetry (O_h) and with a crystal field strength of $10Dq$ = 1.5 eV, and exchange splitting parameter Δ = 3 eV was chosen for the Co ions. The

best spectral reproduction for the Ni L edge was obtained using a crystal field splitting parameter $10Dq$ = 1.5 eV in O_h symmetry and an exchange splitting parameter of Δ = 1 eV for both Ni^{2+} and Ni^{3+} ions. The calculated Co spectra were broadened using a Gaussian with full width at half-maximum of 0.4 eV to account for the experimental broadening at the Co L edge.

Unless specified otherwise, the intensity of all of the photoemission spectra and X-ray absorption spectra were normalized to [0, 1], with the lowest intensity being set to 0 and the highest intensity set to 1. The resonant photoemission spectra were normalized to the intensity of the O 2p emission line.

Conductivity relaxation (CR) measurements were performed in a glass recipient inside a tube furnace in a 2-probe geometry at a temperature of 340 °C. The oxygen partial pressure was controlled via gas mixtures of pure oxygen (pO_2 = 1 bar) and pure nitrogen ($pO_2 \approx 10^{-5}$ bar). CR experiments were performed on the same samples used for the in situ XPS investigations, prior to the spectroscopy experiments. The atmosphere in the furnace can be changed in a few seconds by using several mass flow controllers in parallel, such that the observed relaxation of the current is determined by the oxygen exchange kinetics of the sample and the corresponding change in conductivity upon reduction or oxidation.

■ RESULTS

Surface Oxygen Exchange Kinetics Deduced from Electrical Conductivity Relaxation (ECR). Electrical conductivity relaxation (ECR) is a useful technique to investigate the kinetics of oxygen surface exchange, k^q, and chemical diffusion coefficient, D^{chem}, for oxide materials that are predominantly electronic conductors[16] and has been successfully used on mixed electronic−ionic conductors like BSCF.[17] Because the conductivity of oxide materials is very sensitive to the amount of oxygen vacancies or interstitials in the lattice, the relaxation of electrical conductivity upon a change in the oxygen partial pressure, pO_2, can be used to monitor the oxidation/reduction kinetics. However, ECR is not well suited to the investigation of very thin films because robust results can best be obtained for samples that show a conductivity relaxation that is determined in similar amounts by oxygen surface exchange and diffusion. Because of the very small thickness of the films investigated in this study (5−25 nm), the ECR is dominated by the surface exchange coefficient k^q.[18]

We will therefore use ECR only qualitatively in this study to compare the relaxation kinetics of two samples, a 5 nm NNO film grown on STO (denoted NNO throughout this article) and a 5 nm NNO film grown on a 20 nm LSC film (denoted NNO/LSC in this article). We note that under the same experimental conditions the change in conductivity is much larger in NNO than in LSC and further that the difference in thickness is negligible with regard to the importance of diffusion in this experiment. Using an insulating substrate such as STO at moderate temperatures, the measured conductivity is equal to that of the thin film alone.

Overstoichiometric NNO accommodates excess oxygen in interstitial sites located between the NdO rocksalt layers. The positive charge necessary to balance the negative charge of these interstitials is located on the Ni ions and can migrate to conduct electric current

$$Nd_2^{3+}Ni^{2+}O_4^{2-} + \delta O^{2-} + 2\delta h^{\bullet} = Nd_2Ni_{1-2\delta}^{2+}Ni_{2\delta}^{3+}O_{4+\delta}$$

(1)
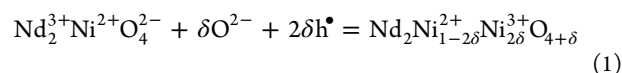
The conductivity of overstoichiometric NNO increases with increasing δ and therefore with increasing pO_2. Figure 2 shows
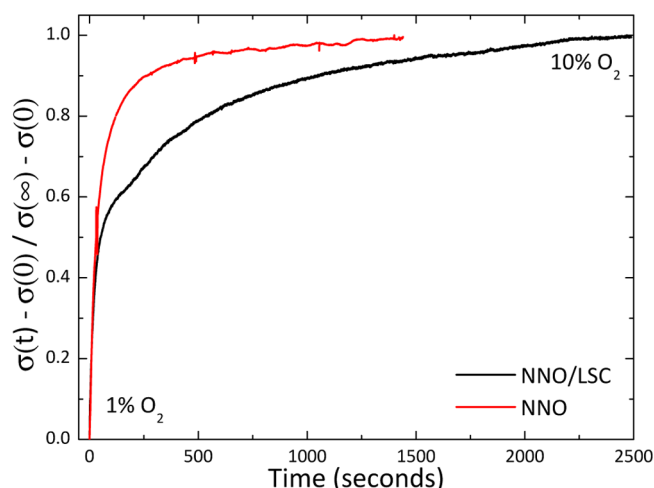

Figure 2. Conductivity relaxation upon the transition from 1% O_2 in N_2 to 10% in N_2 for NNO (red line) and NNO grown on LSC (black line).

conductivity relaxation experiments at 340 °C on a 5 nm thin NNO film (red line) and a 5 nm thin NNO film grown on a 20 nm film of LSC (black line). To better compare the relaxation kinetics, the current has been normalized to account for the different conductivities of the two samples according to the usual procedure.[16] Upon switching the atmosphere from 1% O_2 in N_2 ($pO_2 \approx 10^{-2}$ bar) to 10% O_2 in N_2 ($pO_2 \approx 10^{-1}$ bar), the conductivity of both samples increases in accordance with the oxidation of the samples and an increase in δ. However, the kinetics of this oxidation is very different for the two samples: the conductivity response of the NNO layer on LSC is much slower than that of the reference NNO layer. The same behavior is seen for reduction (data not shown). This suggests that the oxygen exchange kinetics of the NNO/LSC heterostructure is much slower than that of NNO. This effect will be investigated by in situ spectroscopy in the following sections.

Electronic Structure of $Nd_2NiO_{4+\delta}$. As a first step, the electronic structures of NNO and LSC are examined via XAS and RESPES experiments. Consecutively, the same experiments are utilized to examine the electronic structure of the NNO/LSC heterostructure to determine whether a physical reason for the slower ORR kinetics can be identified.

According to eq 1, the valence state of the Ni ions can be conveniently used to determine the oxygen stoichiometry of the material. In Figure 3, the Ni $L_{2,3}$ edge spectrum of a NNO film grown on a STO single crystal is shown (black, open circles), recorded at a temperature of 300 °C and an oxygen pressure of $pO_2 = 10^{-2}$ Torr, along with the calculated Ni^{2+} (blue line) and Ni^{3+} (green line) spectra. A linear combination of 59 ± 2% Ni^{2+} and 41 ± 2% Ni^{3+} (red line) produces a good quantitative reconstruction of the experimental spectrum. We stress that we do not attempt to investigate the electronic configuration of the Ni ions in detail but are instead interested in a reconstruction of the spectrum to quantify the oxygen stoichiometry.
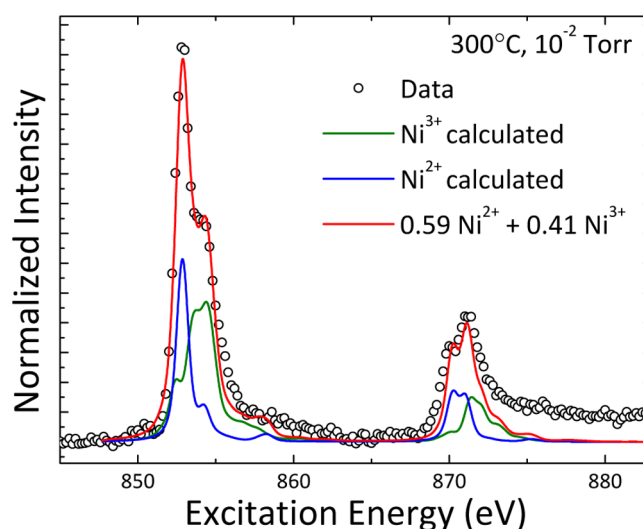

Figure 3. Ni $L_{2,3}$ edge experimental spectrum (black circles) of $Nd_2NiO_{4+\delta}$ recorded at $T = 300$ °C and $pO_2 = 10^{-2}$ Torr. A linear combination of the Ni^{2+} (blue line) and Ni^{3+} (green line) spectra calculated using CTM4XAS can be used to reproduce the spectral envelope (red line).

According to eq 1, the amount of interstitial oxygen is half that of the Ni^{3+} concentration. For the spectrum shown in Figure 3, the oxygen overstoichiometry is therefore $\delta = 0.205$, in good agreement with former investigations of NNO.[19] We point out that this number is not the result of a least-squares fit but rather the result of a spectral reconstruction based on calculated model spectra using the CTM4XAS software package. The agreement between our estimation and known values for the overstoichiometry is nevertheless encouraging.

To determine the influence of the B-site Ni ions on the valence band structure of NNO, resonant photoemission experiments were performed at the Ni $L_{2,3}$ absorption edge, shown in Figure 4 for the same sample. Because the resonant excitation of the $2p \rightarrow 3d$ transition increases the density of states related to the respective 3d orbitals, the valence band spectra are expected to show increased intensity of the features
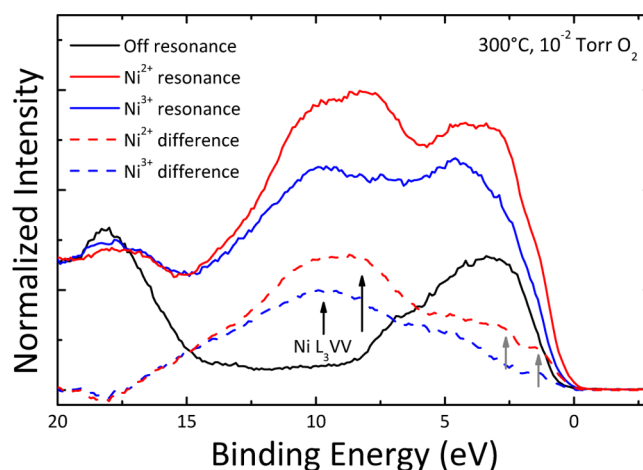

Figure 4. Resonant photoemission spectra of the valence band of NNO, using three excitation energies: off-resonance (black), Ni^{2+} (red) and Ni^{3+} (blue) resonance. The difference spectra between the normalized off- and on-resonance spectra are shown in dashed lines for Ni^{2+} (red) and Ni^{3+} (blue).

related to the 3d orbitals. The RESPES spectra correspond to the excitation energies ($h\nu$) of 845 eV (off-resonance, black), 853 eV (Ni^{2+} resonance, red), and 854.5 eV (Ni^{3+} resonance, blue). The spectra have been scaled such that the intensity coincides at the O 2s core level around 20 eV. Note that this scaling qualitatively preserves the intensity increase observed for the raw spectra, i.e., the Ni^{2+} resonance produces the highest overall intensity in the valence band.

A closer examination of the difference spectra between on-resonance and off-resonance (dotted red and blue lines for Ni^{2+} and Ni^{3+}, respectively) reveals two distinct shoulders close to the Fermi level (marked by the gray arrows), which are more distinct in the Ni^{2+} resonance. We can therefore ascribe these two features to the Ni 3d−O 2p hybridized contributions to the valence band,[20] in agreement with previous studies.[21] The resonant feature closest to the Fermi level is located at $E_{bind} \approx$ 1.4 eV. The strong intensity enhancement below the valence band (marked with black arrows) is a contribution from the Ni L_3VV Auger relaxation process with a kinetic energy of $E_{kin} =$ 844.8 eV, which involves an L_3 core hole and relaxation of electrons from the valence band.

Electronic Structure of $La_{0.8}Sr_{0.2}CoO_{3-\delta}$. To get a reference point for the anionic defect chemistry of the LSC surface under the investigated conditions, we examined a 5 nm LSC layer grown epitaxially on a STO single crystal. Figure 5
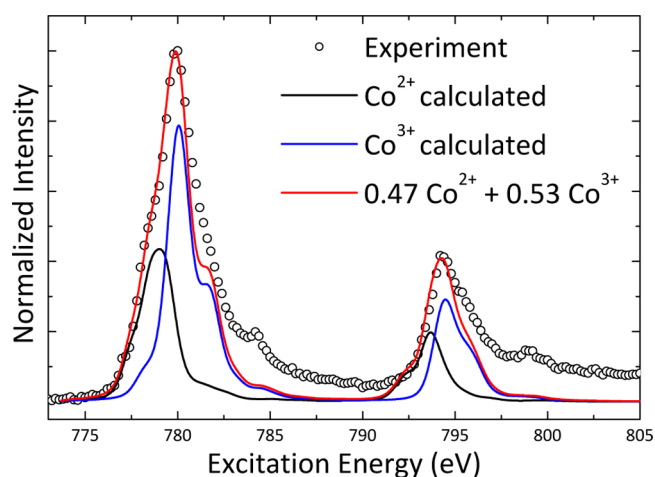

Figure 5. Experimental Co $L_{2,3}$ edge spectrum recorded at 300 °C and $pO_2 = 10^{-2}$ Torr (open circles), along with the spectra calculated by CTM4XAS to represent the Co^{2+} (black line) and Co^{3+} (blue line) contributions and a linear combination of the two calculations (red line).

shows the Co $L_{2,3}$ edge spectrum recorded under experimental conditions (300 °C, 10^{-2} Torr O_2) as black circles and the two calculated spectra representing the contribution from Co^{2+} (black line) and Co^{3+} (blue line) ions. The spectral reconstruction suggests that a significant amount of Co present in the surface region accessible by XAS is reduced to the divalent state (Co^{2+}). The surface of perovskite oxide thin films is often strongly oxygen deficient,[22−25] which is also evidenced in this study through the strong contribution of Co^{2+} ions in the surface.

After normalization and subtraction of a linear background, integration of the L_3 and L_2 lines of the Co $L_{2,3}$ edge spectrum shown in Figure 5 yields the branching ratio = $I_{L_3}/(I_{L_3} + I_{L_2})$ = 0.74, indicating a high-spin configuration of the Co ions.[26]

RESPES at the Co $L_{2,3}$ edge performed on the same sample yielded a resonant photoemission spectrum of the valence band shown in Figure 6. Similar to that in the Ni L edge resonance
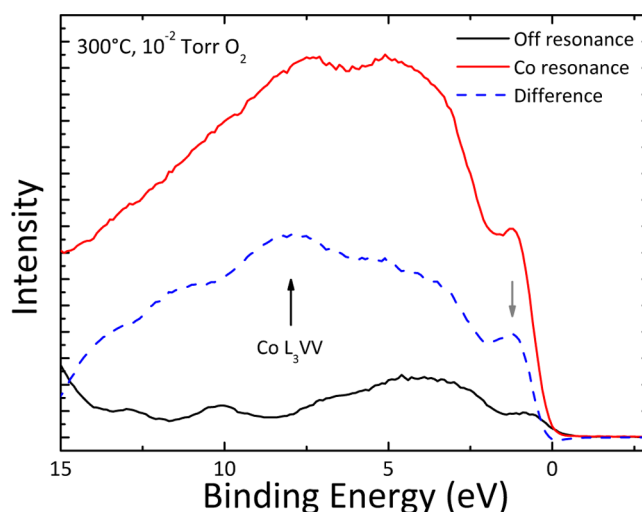

Figure 6. Resonant photoemission spectra of the valence band of LSC grown on a STO_3(001)-oriented single crystal, using two excitation energies: off-resonance (black) and Co^{3+} resonance (red). The difference spectrum between the off- and on-resonance spectra is shown by a dashed blue line.

on NNO, there is a broad contribution from the Co L_3VV Auger process around $E_{bind} = 8$ eV, indicated by the black arrow. In addition, a strong enhancement of the leading edge of the valence band is visible in the resonant spectrum recorded at an excitation energy ($h\nu$) of 779.9 eV (red line), corresponding to the contribution of the hybridized Co 3d−O 2p orbitals to the valence band. When a difference spectrum (dashed blue line) is calculated by subtracting a reference spectrum (recorded off-resonance at $h\nu = 775$ eV (black line)) from the resonant spectrum, it is clearly visible that the maximum of the intensity enhancement is located at approximately $E_{bind} \approx$ 1.25 eV (indicated by the gray arrow).

Charge Transfer in NNO/LSC Heterostructures. In situ X-ray absorption spectroscopy (XAS) and photoemission spectroscopy (XPS) experiments at elevated temperatures and oxygen partial pressures in the range from 10^{-6} to 1 Torr were performed on epitaxial heterostructures to investigate the interaction between the perovskite and RP layers. In particular, resonant photoemission spectroscopy (RESPES) at the Co L edge was used to demonstrate the charge transfer from the perovskite into the RP layer.

Figure 7a shows the Co L edge spectra collected through the 5 nm thin NNO layer. Valence band spectra were recorded at excitation energies ($h\nu$) of 775 eV (off-resonance, marked with a dashed black line) and 780.2 eV (Co L_3 resonance, dashed red line). The resulting valence band spectra are shown in Figure 7b. The spectrum at Co L_3 resonance (red line) shows a clear shoulder at the Fermi level, as well as an overall increase in intensity over the off-resonance spectrum (black line). The difference spectrum (dotted red line) shows a pronounced peak in the NNO valence band situated just below the Fermi level that is related to the Co excitation, as well as a broad spectral feature that can be attributed to the Co L_3VV Auger process.

The two sharp lines located at 784 and 800 eV excitation energies in Figure 7a can be identified as the Ba $M_{4,5}$ edge and
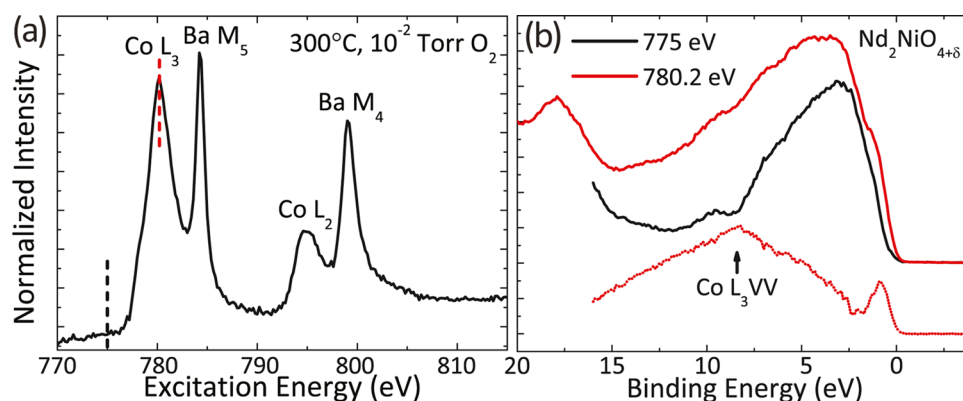
Figure 7. a) Co L edge spectra recorded on the NNO/LSC heterostructure at 300 °C and $pO_2 = 10^{-2}$ mTorr. The black and red dashed lines mark the off- and on-resonance energies, respectively. (b) Valence band spectra of NNO/LSC, with off- and on-resonance (black and red lines, respectively) excitation energies at the Co L_3 edge. The dotted red line shows the difference spectrum.

are the result of a small Ba contamination most likely of the NNO. Going by a simple intensity comparison between the Nd 4d and Ba 4d emission lines, the amount of Ba is less than 2% with respect to the A-site cations. Furthermore, RESPES experiments at the Ba M_5 edge show no change in the valence band other than the Co L_3VV Auger peak, indicating that this minor Ba contamination is not involved in the chemical or electronic structure of NNO and LSC through the interface.

The RESPES experiments reveal a clear increase in the intensity of the NNO valence band just below E_F at Co L_3 edge excitation. Even at a photoelectron kinetic energy of nearly 780 eV, the observed increase is too large to be derived from the LSC layer underneath. The inelastic mean free path of a photoelectron with that kinetic energy can be estimated to 17 Å; thus, the NNO layer absorbs ≈95% of the photoelectron intensity of the LSC layer.[27]

The top of the valence band in transition metal oxides is composed of the hybridized metal 3d bands.[20] For Co^{2+} and Ni^{2+} ions, the electronic configurations are $3d^7$ and $3d^8$, respectively, where the unfilled $e_g\uparrow$ bands form the top of the valence band. Comparing the energy positions of the 3d $e_g\uparrow$ bands in the resonantly excited valence band spectra (Figures 4 and 6), we find that the center of the Ni 3d $e_g\uparrow$ band is located at ≈1.4 eV below E_F, whereas the center of the Co 3d $e_g\uparrow$ band is located ≈1.25 eV below E_F. The result is a charge transfer from Co 3d $e_g\uparrow$ states into Ni 3d $e_g\uparrow$ states across the interface, which explains the enhancement of the NNO valence band at resonant Co L_3 excitation. This effect is similar to what has been found for $La_{1-x}Sr_xMnO_3/La_{1-x}Sr_xFeO_3$ interfaces.[2] In situ experiments provide the distinct advantage that the oxidation state of the sample can be investigated in a controlled manner. We have therefore performed XAS experiments at different temperatures (300 and 415 °C) and values of pO_2 ($pO_2 = 10^{-2}$, 10^{-4}, and 10^{-6} Torr), to vary the chemical potential of the gas-phase oxygen, μ_{O_2}, and therefore the oxidation state of the sample in thermodynamic equilibrium with the gas phase. Because the oxygen nonstoichiometry is accommodated by charge carriers localized at the transition metal ions in both LSC and NNO, it is possible to track the oxygen content indirectly by the valence state of the Co and Ni ions, respectively.

Figure 8 shows Ni L edge spectra recorded at selected (T, pO_2) combinations on both NNO/LSC heterostructures and the NNO reference. For clarity, not all collected spectra are shown. The calculated contributions of the Ni^{2+} and Ni^{3+} ions
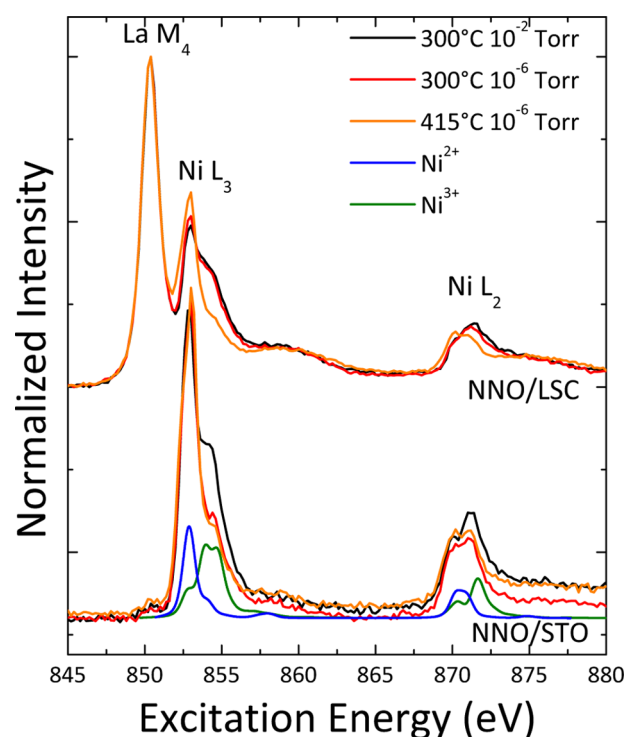

Figure 8. Ni $L_{2,3}$ edge spectra of NNO and NNO/LSC (spectra are offset for clarity) at three different oxygen chemical potentials in the gas phase, defined by (T, pO_2) combinations. NNO/LSC spectra show a contribution from the La M_4 edge of the underlying LSC layer. Calculated spectra for Ni^{2+} and Ni^{3+} are shown as the blue and green lines, respectively, to illustrate the changes between the spectra.

are shown for reference by the blue and green lines, respectively. The NNO reference exhibits changes between the spectra for all different temperatures and pO_2 values investigated, revealing a decreasing Ni^{3+} concentration with decreasing pO_2 and increasing temperature, indicating that the sample is in equilibrium with the gas phase. In contrast, the NNO/LSC heterostructure shows no change in the XAS spectrum with decreasing pO_2 or increasing T, until significant changes are observed when reducing from $pO_2 = 10^{-4}$ to 10^{-6} Torr at $T = 415$ °C. For the sake of completeness, the corresponding XPS spectra can be seen in Figure S3 in the Supporting Information. It is clear, however, that XAS is more sensitive to changes in the oxidation state of Ni than XPS.

A quantitative analysis of the NNO/LSC heterostructure is complicated because of the presence of the La M_4 edge, but despite the large absorption cross section of the rare-earth ions, the sharp line allows for a simple correction using a reference spectrum recorded on an LSC sample under the same conditions. The corrected spectrum can be reconstructed using a linear combination of the calculated Ni^{2+} and Ni^{3+} spectra (see Figure S4 in the Supporting Information). The analysis for $T = 300$ °C and $pO_2 = 10^{-2}$ Torr yields a Ni^{2+}/Ni^{3+} ratio of 0.48/0.52, which corresponds to an oxygen non-stoichiometry of $\delta = 0.26$, according to eq 1. It is clear that compared with the value of $\delta = 0.205$ established for the NNO reference sample under the same thermodynamic conditions (see Figure 3) the overstoichiometry is increased in the NNO lattice of the bilayer structure.

To examine whether the origin of the difference in oxygen stoichiometry in NNO and NNO/LSC can be traced to LSC, we also investigated the valence states of Co in a 5 nm LSC layer grown on STO and a 5 nm LSC layer on 20 nm NNO. A comparison of the Co $L_{2,3}$ edge spectra recorded on LSC/STO and LSC/NNO under the same conditions ($T = 300$ °C and $pO_2 = 10^{-2}$ Torr) yields an almost negligible difference in the spectral weight of the Co^{2+} and Co^{3+} components, as shown in Figure 9. LSC shows the same oxygen stoichiometry under these conditions whether present in the single layer or the bilayer structure, in contrast to the behavior exhibited by NNO. This implies that the additional oxygen interstitials in the NNO/LSC bilayer are primarily integrated into the crystal lattice from gas-phase oxygen.
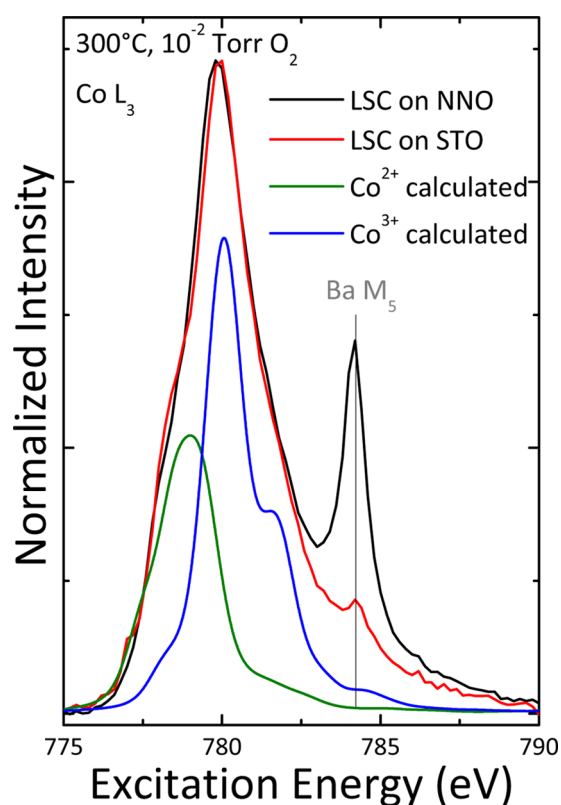

Figure 9. Co L edge XAS spectra recorded at 300 °C and $pO_2 = 10^{-2}$ Torr values on both LSC on STO (red lines) and LSC on NNO (black lines). CTM calculations of Co^{2+} and Co^{3+} ions are shown in blue and green, respectively, to illustrate the spectral weight of the components.

Finally, it is instructive to examine the behavior of the oxygen 1s emission line and the valence band under the same set of thermodynamic conditions. The O 1s and valence band XPS spectra for both NNO and NNO/LSC recorded at an excitation energy ($h\nu$) of 735 eV are shown in Figure 10.
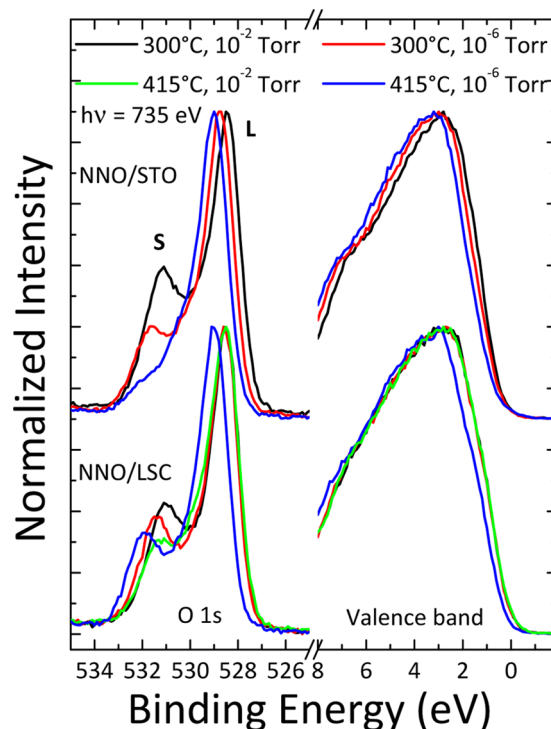

Figure 10. XPS spectra of the O 1s emission line and the valence band for NNO/STO (top) and NNO/LSC (bottom) for various thermodynamic conditions (spectra are offset for clarity). The O 1s emission line shows components corresponding to the lattice oxygen of NNO (marked **L**) and adsorbed surface species (marked **S**).

Analogous to the XAS spectra, the XPS spectra of NNO show distinct changes between the different (T, pO_2) conditions. In particular, a downward shift of the valence band edge for decreasing pO_2 and a corresponding shift of the binding energy of the lattice oxygen emission line (marked **L**) can be observed. The O 1s surface component (marked **S**) shifts in energy as well and decreases in intensity with decreasing pO_2, implying that this line corresponds to oxygen adsorbed on the surface of NNO. The downward shift in binding energy can be explained by a shift of the Fermi energy, E_F, of the system in response to the changing charge carrier concentration, confirming that the NNO sample is indeed in thermodynamic equilibrium.

The NNO/LSC heterostructure behaves somewhat differently, in agreement with the XAS results. Until the most reducing experimental conditions were reached at a temperature of $T = 415$ °C and $pO_2 = 10^{-6}$ Torr, there was no observable change in the valence band or a shift in the binding energy of the lattice component of the O 1s emission line. The binding energy of the adsorbed oxygen species, however, does change in accordance with the pO_2, clearly showing the change of the oxygen chemical potential in the gas phase. At $T = 415$ °C and $pO_2 = 10^{-6}$ Torr, NNO/LSC shows the same downward shift of E_F as NNO/STO. This is in agreement with the Ni L edge XAS spectra recorded under the same conditions, clearly showing a loss of oxygen.

■ DISCUSSION

Coupling the perovskite $La_{0.8}Sr_{0.2}CoO_{3-\delta}$ and the Ruddlesden–Popper phase $Nd_2NiO_{4+\delta}$ via an epitaxial interface has a negative impact on the oxygen exchange kinetics of the surface of NNO, as shown via conductivity relaxation. The resonant photoemission experiments performed under in situ conditions show a Co 2p resonance in the valence band of NNO, a clear indication of a charge carrier transfer across the interface. During in situ investigations of the reducibility, a striking contrast between NNO and NNO/LSC emerges: whereas NNO shows clear evidence of equilibrating with the sample environment, the NNO/LSC heterostructure does not. The binding energy shift of the adsorbed oxygen on the NNO surface provides further evidence because the amount of adsorbed oxygen and the energy position of the emission line clearly correspond to the changing oxygen chemical potential in the gas phase, whereas this is not the case for the NNO/LSC sample. These findings confirm the conclusion of the conductivity relaxation experiments that the oxygen exchange kinetics is far slower or hindered in the NNO/LSC heterostructure, as compared to that in the NNO/STO reference.

Concerning the reducibility of the heterostructure, we find that NNO/LSC does not show significant signs of reduction under the investigated conditions, whereas the oxidation state of Ni in the NNO reference film follows the oxygen chemical potential in the gas phase quite nicely. This is in contrast to previous findings on perovskite/RP systems, where heterostructures based on $La_{1-x}Sr_xCoO_{3-\delta}/(La,Sr)_2CoO_{4+\sigma}$ (LSC113/214) were more easily reducible than the single-phase films.[12] However, a key difference between LSC214 and NNO is that under the investigated conditions, oxygen vacancies are expected to be the dominant defect in $La_{0.5}Sr_{0.5}CoO_4$, whereas oxygen interstitials are expected for NNO, which is in agreement with our findings. Notably, the oxygen reduction kinetics of LSC113/214 heterostructures is accelerated in comparison to that of LSC113 or LSC214, whereas LSC/NNO shows a slower exchange kinetics than that of either NNO or LSC.

Earlier investigations regarding the interaction of perovskite and RP phases across an epitaxial interface concentrate on an enhancement of physical properties.[8,9,28] To fully understand the phenomenon, however, it is necessary to also examine the cases where the opposite effect is observed. Although we do not possess sufficient information about this phenomenon to support an explaining hypothesis, some observations should be pointed out. A key finding of our investigation is that the Fermi level E_F of NNO/LSC does not shift with the oxygen chemical potential, μ_{O_2}, in the continuous way observed for the NNO reference. Because the energy levels of the absorbed oxygen do shift with μ_{O_2}, we can expect that the kinetics of the charge transfer reaction between the solid and the adsorbed oxygen molecule is negatively impacted in the heterostructure.[29]

Because the chemical state of the Co ions in LSC is much less affected by the reducing conditions in our investigation than that of the Ni ions in NNO, it seems reasonable to assume that the improved stability against reduction of the NNO/LSC heterostructure is related to the LSC layer. One possible mechanism causing this effect can be identified as a pinning of the Fermi level of NNO/LSC, which is in turn a likely consequence of the transfer of electronic charge carriers across the interface from the LSC into the NNO layer.

■ SUMMARY

Heteroepitaxial interfaces between perovskite $La_{0.8}Sr_{0.2}CoO_{3-\delta}$ and Ruddlesden–Popper phase $(La,Sr)_2CoO_{4+\delta}$ (LSC214) have been shown to have improved oxygen reduction kinetics compared to that of either LSC or LSC214.[5,7,8] The origin of this phenomenon has been suggested to be related to the exchange of charge carriers and oxygen defects across the interface[9] or interdiffusion of Sr across the interface.[11] To shed further light on this phenomenon, we investigated the heterointerface between $La_{0.8}Sr_{0.2}CoO_{3-\delta}$ and $Nd_2NiO_{4+\delta}$ using electrical conductivity relaxation, in situ X-ray absorption spectroscopy, and photoemission spectroscopy. The reduction kinetics of NNO/LSC heterostructures is negatively impacted compared to that of a NNO reference, as demonstrated by electrical conductivity relaxation experiments. Using in situ photoelectron spectroscopy and X-ray absorption spectroscopy, we find differences between the two systems that are in line with the reduced reduction kinetics. We find clear evidence for electronic charge transfer from LSC into NNO through resonant X-ray photoelectron spectroscopy investigations. The NNO layer in the NNO/LSC film shows a larger oxygen nonstoichiometry compared to that of the single-phase NNO layer, which is likely related to the electronic interaction with the LSC layer. Our results suggest that the charge transfer from LSC to NNO causes a Fermi level pinning in the NNO layer, which results in the decreased oxygen exchange kinetics. Although our findings do not clarify the origin of the enhancement of oxygen exchange kinetics at perovskite/RP interfaces, they demonstrate that the oxygen exchange kinetics of heterointerfaces is sensitive to the chemical composition of the interfacing oxides.

■ ASSOCIATED CONTENT

ⓈSupporting Information

The Supporting Information is available free of charge on the ACS Publications website at DOI: 10.1021/acs.jpcc.7b10284.

Additional information on the sample structure (Figure S1), XPS and XAS analysis depth (Figure S2), Ni 2p XPS spectra (Figure S3), and subtraction of the La M_4 edge from a Ni L edge spectrum (Figure S4) (PDF)

■ AUTHOR INFORMATION

Corresponding Authors
*E-mail: c.lenser@fz-juelich.de (C.L.).
*E-mail: byildiz@mit.edu (B.Y.).

ORCID Ⓞ
Christian Lenser: 0000-0001-5636-2201
Qiyang Lu: 0000-0002-9155-3684
Ethan Crumlin: 0000-0003-3132-190X
Hendrik Bluhm: 0000-0001-9381-3155

Present Address
⊥Institute of Energy and Climate Research (IEK-1), Forschungszentrum Jülich GmbH, 52425 Jülich, Germany (C.L.).

Notes
The authors declare no competing financial interest.

■ REFERENCES

(1) Yildiz, B. "Stretching" the Energy Landscape of Oxides − Effects on Electrocatalysis and Diffusion. *MRS Bull.* **2014**, *39*, 147−156.

(2) Kumigashira, H.; Kobayashi, D.; Hashimoto, R.; Chikamatsu, A.; Oshima, M.; Nakagawa, N.; Ohnishi, T.; Lippmaa, M.; Wadati, H.; Fujimori, A. Inherent Charge Transfer Layer Formation at La$_{0.6}$Sr$_{0.4}$FeO$_3$/La$_{0.6}$Sr$_{0.4}$MnO$_3$ Heterointerface. *Appl. Phys. Lett.* **2004**, *84*, 5353−5355.

(3) Ohtomo, A.; Hwang, H. Y. A High-Mobility Electron Gas at the LaAlO$_3$/SrTiO$_3$ Heterointerface. *Nature* **2004**, *427*, 423−426.

(4) Kushima, A.; Yildiz, B. Oxygen Ion Diffusivity in Strained Yttria Stabilized Zirconia: Where is the Fastest Strain? *J. Mater. Chem.* **2010**, *20*, 4809−4819.

(5) Sase, M.; Hermes, F.; Yashiro, K.; Sato, K.; Mizusaki, J.; Kawada, T.; Sakai, N.; Yokokawa, H. Enhancement of Oxygen Surface Exchange at the Hetero-Interface of (La,Sr)CoO$_3$/(La,Sr)$_2$CoO$_4$ with PLD-Layered Films. *J. Electrochem. Soc.* **2008**, *155*, B793−B797.

(6) Hayd, J.; Yokokawa, H.; Ivers-Tiffée, E. Hetero-Interfaces at Nanoscaled (La,Sr)CoO$_{3-\delta}$ Thin-Film Cathodes Enhancing Oxygen Surface-Exchange Properties. *J. Electrochem. Soc.* **2013**, *160*, F351−F359.

(7) Sase, M.; Yashiro, K.; Sato, K.; Mizusaki, J.; Kawada, T.; Sakai, N.; Yamaji, K.; Horita, T.; Yokokawa, H. Enhancement of Oxygen Exchange at the Hetero Interface of (La,Sr)CoO$_3$/(La,Sr)$_2$CoO$_4$ in Composite Ceramics. *Solid State Ionics* **2008**, *178*, 1843−1852.

(8) Mutoro, E.; Crumlin, E. J.; Biegalski, M. D.; Christen, H. M.; Shao-Horn, Y. Enhanced Oxygen Reduction Activity on Surface-Decorated Perovskite Thin Films for Solid Oxide Fuel Cells. *Energy Environ. Sci.* **2011**, *4*, 3689−3696.

(9) Chen, Y.; Cai, Z.; Kuru, Y.; Ma, W.; Tuller, H. L.; Yildiz, B. Electronic Activation of Cathode Superlattices at Elevated Temperatures − Source of Markedly Accelerated Oxygen Reduction Kinetics. *Adv. Energy Mater.* **2013**, *3*, 1221−1229.

(10) Ma, W.; Kim, J. J.; Tsvetkov, N.; Daio, T.; Kuru, Y.; Cai, Z.; Chen, Y.; Sasaki, K.; Tuller, H. L.; Yildiz, B. Vertically Aligned Nanocomposite La$_{0.8}$Sr$_{0.2}$CoO$_3$/(La$_{0.5}$Sr$_{0.5}$)$_2$CoO$_4$ Cathodes − Electronic Structure, Surface Chemistry and Oxygen Reduction Kinetics. *J. Mater. Chem. A* **2015**, *3*, 207−219.

(11) Gadre, M. J.; Lee, Y.-L.; Morgan, D. Cation Interdiffusion Model for Enhanced Oxygen Kinetics at Oxide Heterostructure Interfaces. *Phys. Chem. Chem. Phys.* **2012**, *14*, 2606−2616.

(12) Tsvetkov, N.; Chen, Y.; Yildiz, B. Reducibility of Co at the La$_{0.8}$Sr$_{0.2}$CoO$_3$/(La$_{0.5}$Sr$_{0.5}$)$_2$CoO$_4$ Hetero-Interface at Elevated Temperatures. *J. Mater. Chem. A* **2014**, *2*, 14690−14695.

(13) Wan, J.; Goodenough, J. B.; Zhu, J. H. Nd$_{2-x}$La$_x$NiO$_{4+\delta}$, a Mixed Ionic/Electronic Conductor with Interstitial Oxygen, as a Cathode Material. *Solid State Ionics* **2007**, *178*, 281−286.

(14) Mauvy, F.; Bassat, J.-M.; Boehm, E.; Manaud, J.-P.; Dordor, P.; Grenier, J.-C. Oxygen Electrode Reaction on Nd$_2$NiO$_{4+\delta}$ Cathode Materials: Impedance Spectroscopy Study. *Solid State Ionics* **2003**, *158*, 17−28.

(15) Stavitski, E.; de Groot, F. M. F. The CTM4XAS Program for EELS and XAS Spectral Shape Analysis of Transition Metal L Edges. *Micron* **2010**, *41*, 687−694.

(16) Lane, J. A.; Kilner, J. A. Measuring Oxygen Diffusion and Oxygen Surface Exchange by Conductivity Relaxation. *Solid State Ionics* **2000**, *136−137*, 997−1001.

(17) Niedrig, C.; Wagner, S. F.; Menesklou, W.; Baumann, S.; Ivers-Tiffée, E. Oxygen Equilibration Kinetics of Mixed-Conducting Perovskites BSCF, LSCF, and PSCF at 900 °C Determined by Electrical Conductivity Relaxation. *Solid State Ionics* **2015**, *283*, 30−37.

(18) Ciucci, F. Electrical Conductivity Relaxation Measurements: Statistical Investigations Using Sensitivity Analysis, Optimal Experimental Design and ECRTOOLS. *Solid State Ionics* **2013**, *239*, 28−40.

(19) Boehm, E.; Bassat, J.-M.; Stevens, P. Oxygen Diffusion and Transport Properties in Non-Stoichiometric Ln$_{2-x}$NiO$_{4+\delta}$ Oxides. *Solid State Ionics* **2005**, *176*, 2717−2725.

(20) Wertheim, G. K.; Hüfner, S. X-Ray Photoemission Band Structure of Some Transition-Metal Oxides. *Phys. Rev. Lett.* **1972**, *28*, No. 1028.

(21) Eguchi, R.; Okamoto, Y.; Hiroi, Z.; Shin, S.; Chainani, A.; Tanaka, Y.; Matsunami, M.; Takata, Y.; Nishino, Y.; Tamasaku, K. Structure and Photoemission Spectroscopy of Strain-Controlled Metal-Insulator Transition in NdNiO$_3$ Thin Films. *J. Appl. Phys.* **2009**, *105*, No. 056103.

(22) Merino, N. A.; Barbero, B. P.; Eloy, P.; Cadús, L. E. La$_{1-x}$Ca$_x$CoO$_3$ Perovskite-Type Oxides: Identification of the Surface Oxygen Species by XPS. *Appl. Surf. Sci.* **2006**, *253*, 1489−1493.

(23) De Souza, R. A.; Gunkel, F.; Hoffmann-Eifert, S.; Dittmann, R. Finite-Size versus Interface-Proximity Effects in Thin-Film Epitaxial SrTiO$_3$. *Phys. Rev. B* **2014**, *89*, No. 241401.

(24) Koehl, A.; Kajewski, D.; Kubacki, J.; Szot, K.; Lenser, C.; Meuffels, P.; Dittmann, R.; Waser, R.; Szade, J. Detection of Fe^{2+} Valence States in Fe-Doped SrTiO$_3$ Epitaxial Thin Films Grown by Pulsed Laser Deposition. *Phys. Chem. Chem. Phys.* **2013**, *15*, 8311−8317.

(25) Cai, Z.; Kuru, Y.; Han, J. W.; Chen, Y.; Yildiz, B. Surface Electronic Structure Transitions at High Temperature on Perovskite Oxides: The Case of Strained La$_{0.8}$Sr$_{0.2}$CoO$_3$ Thin Films. *J. Am. Chem. Soc.* **2011**, *133*, 17696−17704.

(26) Hu, Z. Difference in Spin State and Covalence Between La$_{1-x}$Sr$_x$CoO$_3$ and La$_{2-x}$Sr$_x$Li$_{0.5}$Co$_{0.5}$O$_4$. *J. Alloys Compd.* **2002**, *343*, 5−13.

(27) Tougaard, S. QUASES-IMFP-TPP2M software.

(28) Crumlin, E. J.; Mutoro, E.; Ahn, S.-J.; Jose la O', G.; Leonard, D. N.; Borisevich, A.; Biegalski, M. D.; Christen, H. M.; Shao-Horn, Y. Oxygen Reduction Kinetics Enhancement on a Heterostructured Oxide Surface for Solid Oxide Fuel Cells. *J. Phys. Chem. Lett.* **2010**, *1*, 3149−3155.

(29) Jung, W.; Tuller, H. L. A New Model Describing Solid Oxide Fuel Cell Cathode Kinetics: Model Thin Film SrTi$_{1-x}$Fe$_x$O$_{3-\delta}$ Mixed Conducting Oxides—a Case Study. *Adv. Energy Mater.* **2011**, *1*, 1184−1191.